

Towards Robust Neural Image Compression: Adversarial Attack and Model Finetuning

Tong Chen, *Student Member, IEEE*, and Zhan Ma, *Senior Member, IEEE*

Abstract—Deep neural network based image compression has been extensively studied. Model robustness is largely overlooked, though it is crucial to service enabling. We perform the adversarial attack by injecting a small amount of noise perturbation to original source images, and then encode these adversarial examples using prevailing learnt image compression models. Experiments report severe distortion in the reconstruction of adversarial examples, revealing the general vulnerability of existing methods, regardless of the settings used in underlying compression model (e.g., network architecture, loss function, quality scale) and optimization strategy used for injecting perturbation (e.g., noise threshold, signal distance measurement). Later, we apply the iterative adversarial finetuning to refine pretrained models. In each iteration, random source images and adversarial examples are mixed to update underlying model. Results show the effectiveness of the proposed finetuning strategy by substantially improving the compression model robustness. Overall, our methodology is simple, effective, and generalizable, making it attractive for developing robust learnt image compression solution. All materials have been made publicly accessible at <https://njuvision.github.io/RobustNIC> for reproducible research.

Index Terms—Neural image compression, adversarial example, noise perturbation, model finetuning

I. INTRODUCTION

In past few years, we have witnessed exponential growth of deep neural network (DNN) based image coding approaches. These neural network based image coding (a.k.a., NIC - neural image coding for short) methods [1]–[9] have emerged with outstanding compression efficiency with noticeable gains over conventional solutions like JPEG [10], JPEG 2000 [11], and even the latest Versatile Video Coding (VVC) based Intra Profile (VVC Intra) [12], promising an encouraging prospects of NIC-based applications and services, particularly for those rate-constrained or bandwidth-limited networked scenarios.

Unprecedented coding gains of aforementioned NIC methods mostly came from the introduction of variational auto-encoder (VAE) framework [2], joint entropy context modeling conditioned on both hyperpriors and autoregressive neighbors [4], nonlocal/local attention optimization [6], [7], etc. It was also worth to point out that learning-based NIC offered great flexibility for quickly supporting different image sources, e.g., RGB, YUV, Bayer raw image, etc [13], and for fast enabling the use of a variety of loss functions (quality metrics) [14], [15] in task-oriented applications. On the contrary, it might require substantial efforts to enable additional

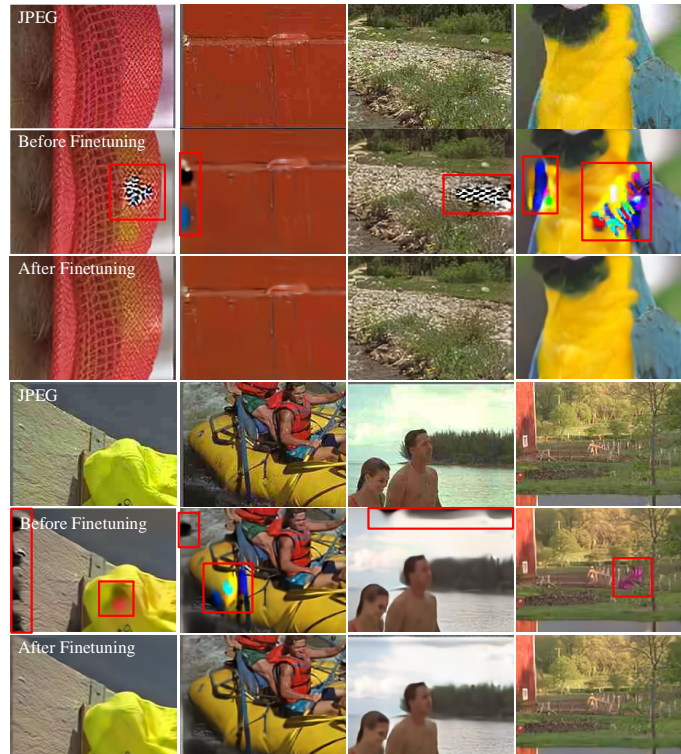


Fig. 1: **Image Recompression.** Row-wisely visual comparison of reconstructions compressed 50 times using JPEG (<http://libjpeg.sourceforge.net/>), pretrained NIC baseline model (a.k.a., Ballé 2018 [2] before finetuning as an example), and the adversarial finetuned NIC model (Ballé 2018 [2] after finetuning). Similar recompression artifacts using learning-based image coder is also reported in [16].

functionalities in traditional image codecs because we had to fully understand the statistical properties of newly-introduced image sources and optimization metrics to develop effective coding toolkit. For example, it took years to facilitate efficient compression of screen content sources when standardizing the extensions of High-Efficiency Video Coding (HEVC).

Recently, after a serial exploration studies, the ISO/IEC JPEG (Joint Photographic Experts Group) committee had made concrete progress on the performance and complexity evaluation of various NIC solutions, and now is initiating the standardization call of next-generation image codec using deep learning techniques. Targeting for the international standard for the interoperability enabling, besides the superior compression efficiency, model robustness/generalization is yet another

T. Chen and Z. Ma are with the School of Electronic Science and Engineering, Nanjing University, Nanjing, Jiangsu, 210093 China. E-mails: tong@smail.nju.edu.cn, mazhan@nju.edu.cn.

critical factor for the potential success of such learnt approach, which however, is often overlooked and not well examined in the past.

Observations. Though rules-based conventional lossy image coding methods, such as the JPEG or VVC Intra would inevitably introduce compression artifacts, yielding visually unpleasant blurring, blocking, ringing impairments in decoded reconstructions. These artifacts mainly deteriorate pixel intensity, whilst the local structure of decoded spatial texture, e.g., edge orientations, are mostly preserved as the input source. However, unexpected pixel impairments would be presented if the image is compressed multiple times using learnt approaches as shown in Fig. 1. Such iterative or successive compression is a common practice for image-based applications over the Internet where images may be re-edited, re-compressed and re-distributed very often. Similar observations are also reported by Kim *et. al* in [16].

Such pixel distortion in decoded image is closely related to the generalization and stability of underlying compression model and is extremely critical for the potential success of NIC solution in practice. This is because the fidelity of compressed image reconstruction plays a vital role in vast applications such as the medical imaging, autonomous self-driving, face recognition, security surveillance, etc. For instance, having incorrect (unexpected) spatial textures in decoded image may lead to very different outcomes of a specific task (e.g., classification) [17] (see Fig. 12), or may also present annoying/disturbing artifacts [16] with severely-degraded user experience (see Fig. 3).

Approach. Recent attempt in [16] investigated the instability of successive deep image compression. However, such instability is not solely with the image recompression task. A systematic stability and generalization evaluation of popular VAE based compression models on full resolution image datasets still remains untouched and is urgently needed for the pursuit of robust NIC.

Unfortunately, it is almost impossible to manually analyze and search for all potential cases that may cause model instability. As inspired by emerged popular adversarial attack studies on high-level vision tasks like classification [18]–[20], semantic segmentation [21] and object detection [22], and low-level tasks like super resolution [23] and optical flow derivation [24] to respectively examine their model robustness, we suggest to automatically generate adversarial examples to attack the NIC models used for image compression, analyze the impacts on coding efficiency and reconstruction quality (quantitatively and qualitatively), exploit the insights behind, and develop effective solutions to defend these attacks.

Hence, we try to optimize the generation of adversarial examples with only a small amount of almost negligible perturbation added to the original source images but lead to severe distortion in the corresponding reconstruction, with which we can examine the instability of existing NIC methods. Such adversarial attack is referred to as the “untargeted” attack without designated purpose that particularly aims for misleading the semantic understanding of the reconstructed content. In Sec. VI, we also demonstrate how targeted attack can affect the reconstruction of NIC methods.

TABLE I: Frequently Used Abbreviations

Abbreviation	Description
NIC	Neural Image Compression
JPEG	Joint Photographic Experts Group
VVC	Versatile Video Coding
MSE	Mean Squared Error
PSNR	Peak Signal-to-Noise Ratio
MS-SSIM [14]	Multscale Structural Similarity
LPIPS [25]	Learned Perceptual Image Patch Similarity
bpp	bit rate using bits per pixel
GAN	Generative Adversarial Network
VAE	Variational AutoEncoder

Later we leverage generated adversarial examples to iteratively finetune the original models, improving the robustness of NIC to adversarial attacks. We also show that adversarial finetuned model can effectively eliminate the distortions induced by image recompression as in Fig. 1.

Contribution.

- 1) To the best of our knowledge, this is the first work that performs adversarial attack to systematically study the model instability of learnt image compression on full resolution images (Sec. III);
- 2) Our extensive experiments report the general vulnerability of existing learning-based image compression method regardless of the underlying model settings and perturbation generation strategy (Sec. IV);
- 3) The proposed iterative adversarial finetuning simply augments the original training dataset with adversarial examples to finetune the existing compression model, by which it not only improves the model robustness substantially but also retains most of the original compression efficiency (Sec. V);

Overall, our methodology that includes the noise injection based adversarial example generation, and adversarial model finetuning using generated examples, is simple, effective and generalizable to most popular learnt image coder approaches, making it attractive and necessarily desired for practical application.

II. RELATED WORKS

This section briefs relevant techniques on respective lossy image compression and adversarial attack.

A. Lossy Image Compression

Lossy image compression approaches, such as the JPEG [10], JPEG 2000 [11], VVC Intra, etc, usually search for appropriate compact representation through rate-distortion optimization (RDO). Typically solutions often adopt the “transform coding” or “hybrid transform/prediction coding” to transform input pixels, or pixel residuals (after intra prediction) into frequency domain coefficients for quantization and entropy coding. These transforms are generally comprised of a set of basis functions that are weighted to represent arbitrary pixel-domain blocks/patches using a few sparse, nonzero coefficients.

Classical Methods. Classical transforms include Discrete Cosine Transform (DCT) [28], Wavelet Transform [29], and so

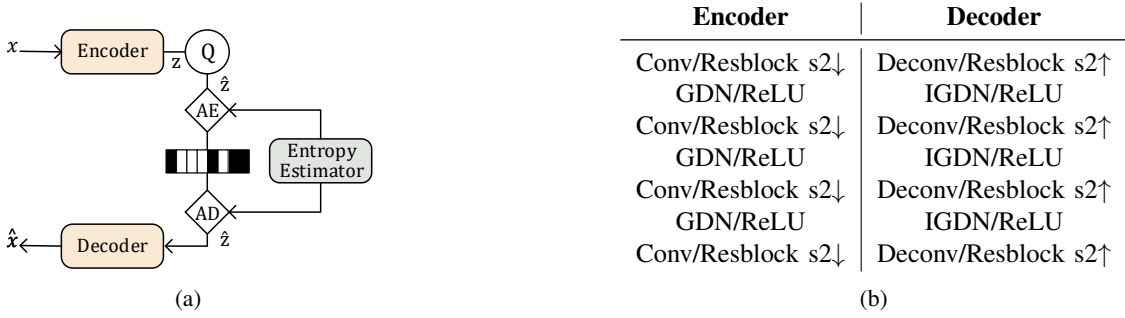


Fig. 2: **Neural Image Compression (NIC)**. (a) General architecture of VAE-based NIC Solutions. Q denotes the quantization, and entropy estimator provides the probability estimation for both AE (Arithmetic Encoding) and AD (Arithmetic Decoding); x is an original source image (or input source), and correspondingly \hat{x} is the output reconstruction (after decoding). (b) Typical paired Encoder and Decoder components used in NIC framework, such as normal Convolutional layer (Conv) or ResNet block (Resblock) [26], resolution re-sampling (upsampling $s2\downarrow$ and downscaling $s2\uparrow$ at a factor of 2), nonlinear activations using GDN (Generalized Divisive Normalization) [27] or ReLU (rectified linear unit). Deconv and IGDN are inverted processes of respective Conv and GDN.

on. Taking DCT as an example, its transform coefficients are usually clustered at few low-frequency components which can be leveraged for energy compaction. The DCT is invertible, i.e., the original image x can be reconstructed losslessly by applying the inverse DCT (IDCT), e.g., $x = f_{\text{dct}}^{-1}(f_{\text{dct}}(x))$. Here f_{dct} and f_{dct}^{-1} are DCT and IDCT respectively.

Over-complete Dictionary. Image data typically exhibits non-stationary behavior, making it difficult to be de-correlated sufficiently by existing DCT or wavelets. Dictionary learning is then introduced to use a number of content-adaptive, over-complete dictionary atoms to represent image blocks using more sparse and easy-to-compress coefficients [30], [31].

Neural Transform. Built upon its excessive representation capacity of high-dimensional data, deeply stacked convolutional neural networks (CNNs) are therefore utilized to construct neural transforms to represent image blocks in a more compact representation (see Fig. 2b). Fig. 2a plots a popular VAE architecture that applies neural transform and successfully demonstrates superior coding efficiency [1], [2], [4], [6], [7], [32].

The forward transform in encoder analyzes the original image source x and represents it using compact, vectorized latent features z for quantization (e.g., $\hat{z} = Q(z)$) and entropy coding with learnt adaptive contexts. Oppositely, the backward transform in decoder mirrors the forward steps in encoding process to generate the reconstruction \hat{x} . As usual, the RDO module controls the compression trade-off, e.g.,

$$R + \lambda D = \underbrace{\mathbb{E}[-\log_2 p(\hat{z})]}_{\text{rate}} + \lambda \underbrace{\mathbb{E}\|x - \hat{x}\|_2^2}_{\text{distortion}}, \quad (1)$$

with $p(\hat{z})$ standing for the symbol probability of feature elements at bottleneck layer [7].

Unlike DCT or wavelet transform, forward neural transform $f_E()$ in encoder and its inverse presentation $f_D()$ in decoder are non-linear functions, and usually not invertible even without quantization error,

$$x \neq f_D(f_E(x)). \quad (2)$$

Even having invertible neural transform as studied in [33], [34], the quantization error may also be amplified during decoding for lossy compression. For either case, $f_D()$ and $f_E()$ are made up of a stack of convolutional layers that consist of linear convolution, activation function, and possible spatial re-sampling (or spatial-channel shuffling), with which it would potentially amplify any perturbation through layer-by-layer computation and lead to unexpected impairments. As explained in previous work [18], linear behavior in high-dimensional spaces is sufficient to cause the vulnerability of deep neural networks against adversarial examples, implying that deep neural transform based NIC methods are very possibly vulnerable to input perturbation.

B. Adversarial Attack

Adversarial attacks have been widely utilized to measure the robustness of DNN models in various approaches, particularly for those in high-level vision tasks as aforementioned. As known, these DNN models basically wish to construct non-linear mapping function g to effectively characterize the relationships between input data and output result.

Adversarial attack can be either *targeted* or *untargeted*. Given a vectorized input x and a mapping function $y = g(x)$, for *untargeted* attack, adversarial examples x^* are used to produce undesigned but incorrect output. They can be derived using:

$$\underset{x^*}{\operatorname{argmin}} d\{x, x^*\} \text{ s.t. } g(x^*) \neq g(x). \quad (3)$$

Here $d\{\cdot\}$ measures the signal distance between original x and adversarial example x^* , for which conventional MSE or other metrics can be used.

Adversarial attack can be also *targeted*. Having an image classification example, a targeted attack, as the name implies, attempts to use example x^* that has only limited perturbation compared with original input x , to “fool” the classifier f to mis-classify x^* to some targeted label $y^t = f(x^*)$ that is

TABLE II: Tested NIC Approaches and Their Key Components.

Method	Key Components		
	Nonlinear Transform	Entropy Model	Loss
Ballé 2016 [1]	Conv+GDN	factorized	MSE / MS-SSIM
Ballé 2018 [2]	Conv+GDN	hyperprior	MSE / MS-SSIM
Minnen [4]	Conv+GDN	joint hyperprior & autoregressive	MSE
Cheng 2020 [6]	Resblock+Spatial-Channel Attention	joint hyperprior & autoregressive	MSE
NLAIC [7]	Resblock+Nonlocal Attention	joint hyperprior & autoregressive	MS-SSIM
HiFiC [5]	Conv+Channel Normalization	hyperprior	MSE + LPIPS [25] + GAN
Weixin 2021 [35]	Fixed-point NLAIC	joint hyperprior & autoregressive	MSE
InvCompress [34]	INN+Attention+Feature Enhancement	joint hyperprior & autoregressive	MSE

totally different from the original outcome y . Such targeted adversarial examples can be generated through:

$$\operatorname{argmin}_{\mathbf{x}^*} d\{\mathbf{x}, \mathbf{x}^*\} \text{ s.t. } f(\mathbf{x}^*) = y^t. \quad (4)$$

Many popular methods like stochastic gradient decent (SGD), Adam [36] and fast gradient-based techniques like FGSM [18] can be used for solving (3) and (4) automatically.

Existing attempts of adversarial attacks on VAE-based methods [37], [38] only focus on generative models like VAE-GAN [39] and mainly use very low-resolution (e.g. 28×28), simple digital number datasets like MNIST and SVHN [40]. To the best of our knowledge, there has been no existing work on attacking full resolution image compression framework. As aforementioned, the stability of decoded reconstruction in image compression tasks is critical to applications. Thus we hope to see, whether limited perturbations in input can produce unexpected distortion on the output image after compressed by NIC methods. Technically, this is an untargeted attack. Therefore, this work will first demonstrate how existing image compression models can be affected by the untargeted attack and how to defend them for robust image compression. Later then, we also show that our methodology can be easily extended to targeted attack.

III. ADVERSARIAL EXAMPLES

Images are mostly compressed for vast applications due to rate/bandwidth constraints in practice. The compression technology behind is mandated to guarantee the interoperability across heterogeneous platforms, client devices, etc, which is often presented as an international standard or industrial recommendation that is reproducible and publicly accessible. Hence, we generally assume that the attacker can have the full access of the NIC codec and model parameters to best generate adversarial examples for attack [38]. So technically the proposed attack belongs to *white-box* attack.

Without making any modification of the pretrained encoder $f_E()$ and decoder $f_D()$ of a specific NIC method, the attacker wishes to inject a small amount of noise \mathbf{n} upon the original source image \mathbf{x} to generate the adversarial example (or input) $\mathbf{x}^* = \mathbf{x} + \mathbf{n}$. These images are respectively encoded and decoded to have adversarial reconstructions $\hat{\mathbf{x}}^* = f_D(f_E(\mathbf{x}^*))$, and original reconstructions $\hat{\mathbf{x}} = f_D(f_E(\mathbf{x}))$. The generated \mathbf{x}^* should have only limited or negligible perturbation compared with the original input \mathbf{x} , while the decoded adversarial reconstruction $\hat{\mathbf{x}}^*$ of the adversarial input \mathbf{x}^* is expected to largely differ from the reconstruction $\hat{\mathbf{x}}$ of original \mathbf{x} with

visible distortion. Therefore, the adversarial examples for such untargeted/distortion attack can be derived by optimizing the added noise \mathbf{n} with:

$$\operatorname{argmin}_{\mathbf{n}} L_d = \begin{cases} \|\mathbf{n}\|_2^2, & \|\mathbf{n}\|_2^2 \geq \epsilon, \\ 1 - \|\hat{\mathbf{x}} - \hat{\mathbf{x}}^*\|_2^2, & \|\mathbf{n}\|_2^2 < \epsilon. \end{cases} \quad (5)$$

where ϵ is the l_2 threshold of the input noise.

When augmented noise is strong, e.g., having $\|\mathbf{n}\|_2^2 \geq \epsilon$, the objective function is first to decrease the noise intensity until $\|\mathbf{n}\|_2^2 < \epsilon$; hereafter, we use the negative l_2 distance between the original reconstruction $\hat{\mathbf{x}}$ and adversarial reconstruction $\hat{\mathbf{x}}^*$ to maximize their distance. We preset ϵ to enforce the same level of perturbation added in the input, and maximize the output distortion in the meantime. As seen, we can easily adapt ϵ to get proper adversarial examples as expected. As will be shown in later section, other distance metrics, such as the l_1 distance, structural similarity based MS-SSIM, can be also used to guide the example generation. The proposed perturbation generation strategy in (5) is a general approach that is effective for any NIC models used in practice. As will be shown in later section, these generated adversarial examples can be used for finetuning existing NIC models. The finetuned model can effectively defend the artifacts induced by adversarial attack as well as by practical applications like successive image recompression.

IV. ATTACK EVALUATION

This section follows the optimization strategies proposed in (5) to measure the robustness of the popular NIC methods. Adam [36] optimizer is used to optimize the (5). Extensive simulations reveal that distortion attack works effectively and leads to visible impairments in adversarial reconstruction regardless of underlying NIC methods, noise injection schemes, etc.

A. NIC: Approaches and Settings

1) *General Observation*: We choose a variety of VAE-based NICs shown in Table II to demonstrate the general existence of instability among recently emerged NIC solutions. These NICs exemplify major milestones of key components during the development of learning-based image coding.

Theoretically, image coding efficiency is highly related to the efficiency of nonlinear transform and entropy context modeling. Earlier attempt made in Ballé 2016 [1] first introduced the Generalized Divisive Normalization (GDN) with convolutional layer, and applied simple factorized entropy model that

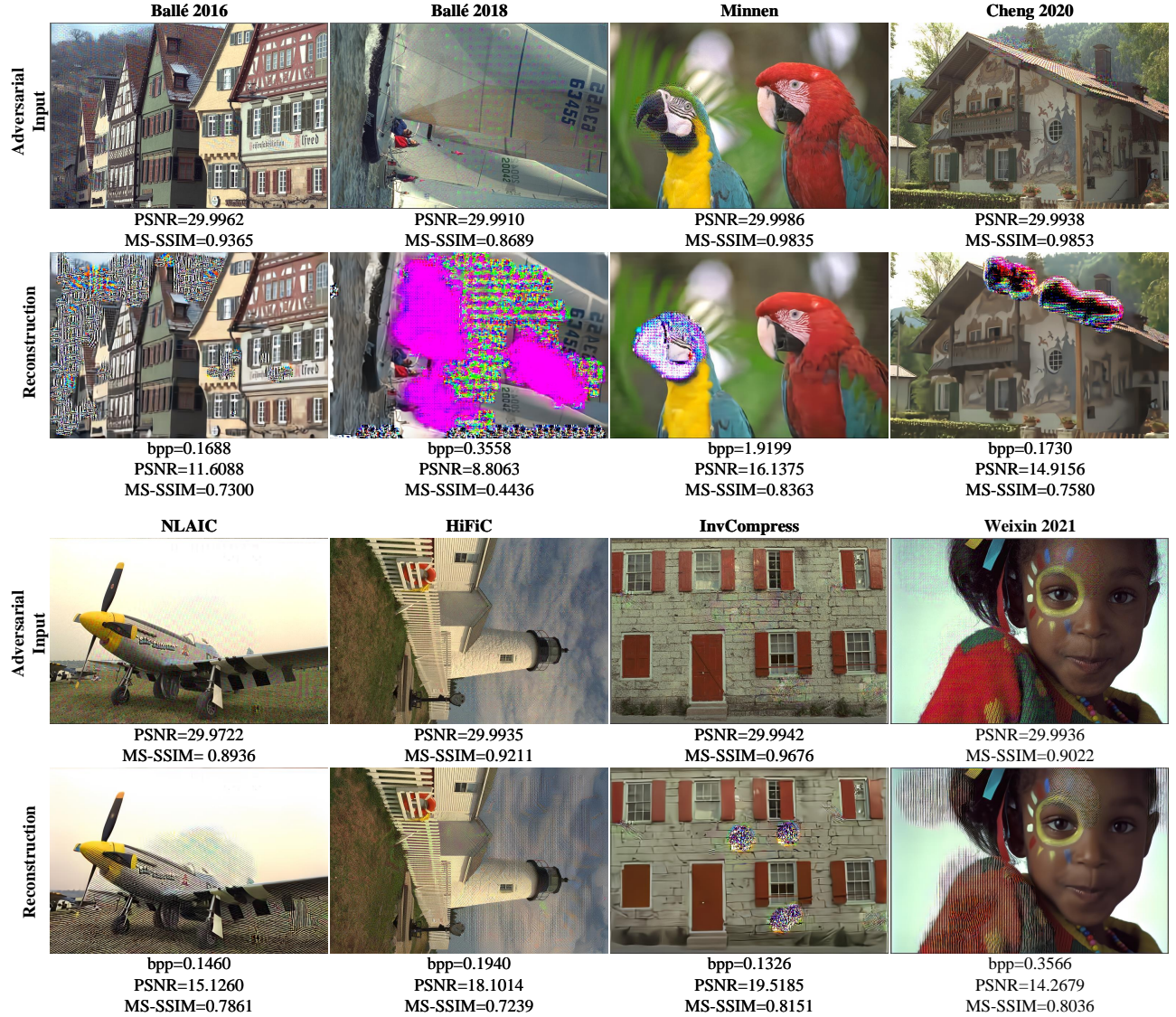


Fig. 3: **Model Instability Incurred Reconstruction Distortions.** Both adversarial inputs and decoded reconstructions are visualized. Input images are compressed using existing NICs listed in Tab. II. The bitrate is measured by bpp (bits per pixel). All PSNR and MS-SSIM values are compared with the uncompressed original image x for quantitative measurement. Such measurement is extended to all other simulations in this study.

TABLE III: Original reconstruction and adversarial reconstruction quality comparison for different NIC methods averaged on Kodak dataset. The “mse” and “ms-ssim” indicate the model optimized using MSE and MS-SSIM loss respectively.

Method	Original		Adversarial	
	PSNR	MS-SSIM	PSNR	MS-SSIM
Ballé2016 (mse)	29.6194	0.9554	17.1008	0.8521
Ballé2016 (ms-ssim)	27.2918	0.9650	11.5161	0.6087
Ballé2018 (mse)	30.9674	0.9609	17.0802	0.8511
Ballé2018 (ms-ssim)	27.1062	0.9706	11.6085	0.6752
Minnen 2018 (mse)	31.3861	0.9627	16.1951	0.8384
Cheng 2020	31.3035	0.9624	20.1133	0.8768
HiFiC	27.0348	0.9217	19.5471	0.7438
NLAIC	27.2177	0.9556	14.3657	0.7317
Weixin 2021	30.3835	0.9748	15.7722	0.8729
InvCompress	31.3094	0.9541	21.3836	0.9266

was further improved in Ballé 2018 [2] and Minnen [4] by hyper prior, and joint hyper prior and autoregressive neighbors for better entropy modeling; Because of the superior efficiency by using joint hyper prior and autoregressive neighbors, succeeding works almost reused the same mechanism in context modeling.

Given that convolution mostly captures the local correlation, NLAIC [7] and Cheng 2020 [6] suggested the attention mechanism to aggregate local or nonlocal correlations to enhance the performance. Previous discussions mainly applied the MSE or MS-SSIM as the loss function in training while HiFiC [5] combined the MSE, LPIPS (Learned Perceptual Image Patch Similarity) and GAN (Generative Adversarial Network) loss to noticeably improve the perceptual quality of reconstructed images.

In addition to the coding efficiency, other aspects were

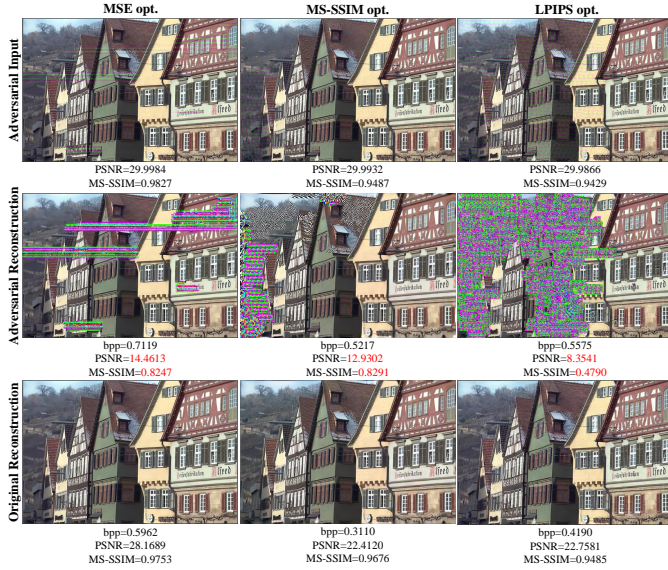


Fig. 4: **Impact of Loss Functions Used for Training NIC.** Illustration of adversarial examples, adversarial reconstructions (via decoding compressed adversarial inputs), and original noise-free reconstructions for three different NIC models optimized using MSE, MS-SSIM and LPIPS respectively. Both PSNR and MS-SSIM are evaluated against the original noise-free input. Compressed bit rates in bpp increase when encoding the adversarial examples that have noise perturbation.

considered as well. For example, aforementioned models with floating point computation were platform dependent and complexity intensive. In Weixin 2021 [35], it developed the fixed point strategy to optimize the NLAIC [7], yielding negligible performance loss but significant complexity reduction. Note that nonlinear transforms in [1], [2], [4], [6], [7] were not invertible and could not avoid the information loss, alternative InvCompress [34] used invertible neural network (INN) as its core transform to resolve this issue.

We generally utilize open-sourced code and pretrained models of these methods (e.g., compressAI¹ [41], NLAIC², Weixin 2021³, HiFiC⁴ and InvCompress⁵) to avoid any ambiguity. For those missing models, we strictly follow the training procedures to reproduce them from scratch.

For fair comparison, the noise threshold ϵ in (5) is set to $1e-3$, having the PSNR between the original image and corresponding adversarial example equal to 30dB. We run 100,00 steps with learning rate at $1e-3$ to generate adversarial inputs for NIC methods listed in Table II using images from Kodak dataset [42]. In Fig. 3⁶, the adversarial inputs and corresponding reconstructions are visualized for each method. Visible impairments are clearly presented in these

¹<https://github.com/InterDigitalInc/CompressAI>

²<https://njuvision.github.io/NIC/>

³<https://njuvision.github.io/fixed-point/>

⁴<https://github.com/tensorflow/compression/tree/master/models/hific>

⁵<https://github.com/xyq7/InvCompress>

⁶We use different images for diverse NIC solutions to exemplify the severe quality degradation of decoded image incurred by the model instability. Such visible distortions are presented for other images as well.

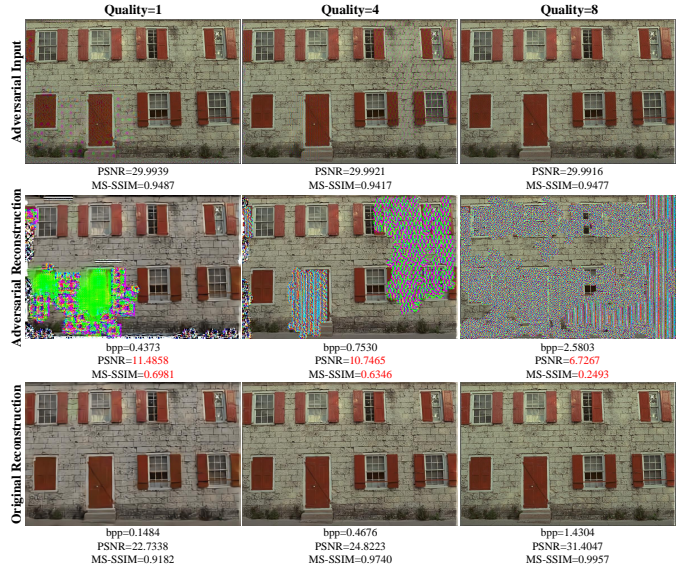


Fig. 5: **Impact of Quality Scales Used in NIC.** Illustration of adversarial examples, adversarial reconstructions and original noise-free reconstructions for three different quality scales used in NIC model. The quality scale parameter in CompressAI is set to [1,4,8] to represent low-quality (e.g., low-bitrate), intermediate-quality and high-quality (high-bitrate) compression.

reconstructions for most popular NICs (even for methods using invertible neural network [34] and fixed-point computation [35]), implying that the instability issue applies to all learning-based image coding frameworks regardless of diverse components and optimization methods utilized. Extremely-low PSNR and MS-SSIM measurements of reconstructions, e.g., < 20 dB, also confirm the aforementioned subjective loss. More numerical comparison results can be found in Table III that lists the reconstruction quality of the original no noise input and of adversarial input averaged on 24 Kodak images. Note that all PSNR and MS-SSIM values are measured against the uncompressed, original image x for quantitative evaluation in this study.

Note that the first three methods Ballé 2016 [1], Ballé 2018 [2] and Minnen 2018 [4] use the same encoder and decoder transform. Their main difference is the entropy estimator used for coding the latent feature (see more details in Table II). As seen in Table III, these methods show clear vulnerability to adversarial attacks regardless of different entropy approximations.

InvCompress [34] that applies the invertible neural network to avoid information loss shows the best adversarial reconstruction quality among all tested methods in Table III. However, the model instability is still presented with obvious distortion in Fig. 3, which might be caused by the use of feature enhancement modules before and after the invertible neural network transforms.

For the sake of simplicity, we then take the classic and most representative Ballé 2018 [2] method as an example in the rest of the article, to systematically evaluate how the adversarial

attack and defense would affect the robustness of learnt image compression.

2) *Loss Functions*: One advantage of learning-based NIC solution to existing rules-based JPEG, VVC Intra, etc, is that we can easily adapt specific loss function towards designated quality optimization. In addition to the traditional MSE (Mean squared error) and MS-SSIM (Structural similarity) that are extensively used in model training, recent works have suggested that LPIPS, feature loss, as well as the GAN loss can be applied separately or jointly for better perceptual quality of decoded reconstructions because these metrics show better correlation with the subjective sensation [25], [43].

We separately optimize the Ballé 2018 [2] using three popular loss functions, e.g., MSE, MS-SSIM, and LPIPS. As illustrated in Fig. 4, model instability incurred distortions are again presented, besides the impairments observed in Fig. 3 for image coded by GAN loss optimized HiFiC, implying successful attacks on underlying NIC model regardless of the loss function used in model optimization. Sharp drops of PSNR and MS-SSIM are noted when quantitatively comparing the reconstruction of compressed adversarial examples at 2nd row to those of compressed inputs without adversarial attack at 3rd row. We also notice that the bit rate measured in bpp increases when compressing the adversarial examples to corresponding attack-free inputs, which reveals that the injected noise is more difficult to model for efficient coding.

3) *Quality Scales*: In practice, images will be encoded at various quality scales (or bit rates) for satisfying diverse application requests. Rate-distortion optimization shows that a larger bit rate would basically come with a better quality scale after reconstruction. However, as shown in Fig. 5, the NIC models are constantly vulnerable to adversarial attacks at all quality scales.

$$\lim_{r \rightarrow +\infty} \|x - f_D(f_E(x))\| = \varphi \quad (6)$$

Actually, due to the irreversibility of VAE-based methods as mentioned in (2), there exists a distortion up-bound or **AE limit** φ in (6) as mentioned in [33] when the bitrate r increases. It explains why it is possible to generate adversarial examples for models trained for arbitrary bitrates.

Along with the increase of compressed bitrate, the quality of adversarial reconstruction gets even worse. It is because, at low bitrates, even though adversarial examples are with the perturbation, higher quantization level would remove more details as well as noises, which could partially stop the noise accumulation and present less distortions. However, when bitrate gets higher, the model tries to retain more information of the input image, which also accumulates the perturbation layer by layer to produce severer distortion.

B. Adversarial Example Generation Settings

Previous sections report that existing NIC models are vulnerable to adversarial attacks regardless of the implementation methods, loss functions, and compressed bitrates utilized. This section further shows that adversarial attack works in general when applying different noise threshold and distance measurement in (5) to inject perturbation.



Fig. 6: **Impact of ϵ** . Illustration of adversarial examples at first row, associated noise at second row and corresponding decoded reconstructions at third row for different perturbation levels. ϵ is adjusted to adapt the intensity of noise for input perturbation, i.e., larger ϵ is for stronger perturbation.

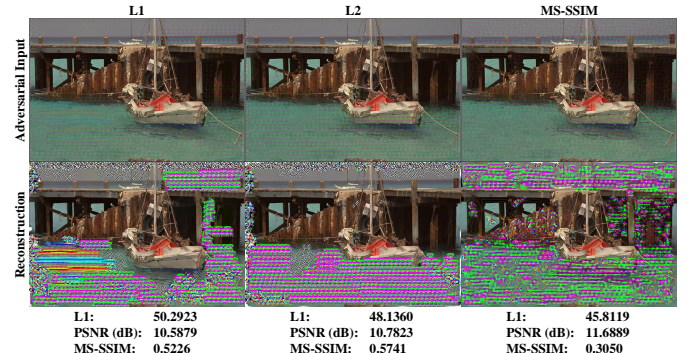


Fig. 7: **Impact of Distance Measurements Used for Generating Adversarial Examples**. Illustration of adversarial examples and corresponding adversarial reconstructed using different distance measurements in (5).

1) *Noise Threshold ϵ* : Figure 6 visualize adversarial examples when having different levels of input perturbation through ϵ adjustment. The results is consistent with the intuition, i.e., larger ϵ leads to stronger noise for input image perturbation, and thus yields more severely-degraded reconstructions. Surprisingly, even with negligible visual artifacts when having $\epsilon = 1e - 5$, impaired pixels are still presented in decoded reconstruction, implying the very vulnerability of NIC models.

2) *Distance Measurement*: We originally apply the common l_2 distance in (5) to optimize the noise injection for

the generation of adversarial examples. Here, we show that l_1 distance and MS-SSIM measurement can be used to produce adversarial examples that can also effectively attack NIC models for impaired reconstructions in Fig. 7.

V. ATTACK DEFENSE

Extensive experiments in last section report that existing NIC models are very vulnerable to adversarial attacks, suggesting that designating different network structures and applying various loss functions cannot successfully defend the attack. The distortion in adversarial reconstructions is incurred possibly because NIC models trained using noise-free dataset is incapable of characterizing noised content with different distribution that was unseen during training. In the meantime, previous works on adversarial training with adversarial examples [19], [44]–[46] have already shown the ability to improve the robustness of the underlying learnt model for various vision tasks. Thus, we suggest to apply the simple yet effective adversarial finetuning strategy to get robust NIC models.

A. Iterative Adversarial Finetuning

Existing NIC approaches often use noise-free (or at least less noise), high-quality, uncompressed image samples to train respective models. They work well on clean and uncompressed content, but are mostly vulnerable to noisy inputs as aforementioned. Experiments in previous sections have shown that such noisy inputs can be simulated by adversarial example generation, we then propose to augment these generated adversarial examples into original training dataset, by which we can basically enrich the distribution of training data for improving the model generalization afterwards.

As described in Algorithm 1, we iteratively implement the *attack-and-finetune* strategy to update the pretrained model. Here θ , ϕ are trainable parameters in encoder $f_E()$ and decoder $f_D()$ respectively. N is the total iterations of adversarial finetuning and in each iteration, a batch of 8 images are randomly sampled from training dataset \mathbb{D} , in which four of them are kept as original images \vec{x}_{ori} and the other four images would be used to generate adversarial examples \vec{x}^* with M steps of optimization following (5). \vec{x}_{ori} and \vec{x}^* is then concatenated together to update the pretrained models with Adam optimizer. In this paper, we set $N = 1000$, $M = 1000$. Randomly-cropped $256 \times 256 \times 3$ patches from DIV2K [47] dataset are used as the training baseline dataset \mathbb{D} . Note that $\epsilon = 1e-3$ and l_2 distance is used. The generation of each batch of adversarial examples costs about 22s on the platform with Intel Xeon Silver 4210 CPU@2.20GHz and single NVIDIA RTX 2080Ti GPU.

B. Defense Efficiency

We mainly show the efficiency of attack defense in two folds: one aspect is about the distortion removal in adversarial reconstructions; and the other one is about the coding efficiency of the adversarially finetuned model. Here, the most vulnerable MS-SSIM optimized Ballé 2018 method is used as an example to demonstrate the defense efficiency.

Algorithm 1 Iterative Adversarial Finetuning

Input: Encoder $f_E()$ parameters θ , Decoder $f_D()$ parameters ϕ , Dataset \mathbb{D} , finetuning iterations N , adversarial example generation iterations M ,

Output: θ^* , ϕ^*

```

1:  $\theta^*, \phi^* = \theta, \phi$  //initialize using pretrained baseline model
2:  $i = 0$ 
3: for  $i < N$  do
4:    $\vec{x}_{\text{ori}} = \text{RANDOM\_SAMPLE\_FROM}(\mathbb{D}, \text{batchsize}=4)$ 
5:    $\vec{x}_{\text{adv}} = \text{RANDOM\_SAMPLE\_FROM}(\mathbb{D}, \text{batchsize}=4)$ 
6:    $j = 0, \mathbf{n} = \text{RANDOM\_NOISE}(), \vec{x}^* = \vec{x}_{\text{adv}} + \mathbf{n}$ 
7:   for  $j \leq M$  do
8:     optimize  $\vec{x}^*$  by Eq. (5)
9:      $j = j + 1$ 
10:  end for
11:   $\vec{x}_{\text{new}} = [\vec{x}_{\text{ori}}, \vec{x}^*]$ 
12:   $dloss = \text{DISTORTION\_FUNCTION}(f_D(f_E(\vec{x}_{\text{new}})), \vec{x}_{\text{new}})$ 
13:   $rloss = \text{RATE\_FUNCTION}(f_E(\vec{x}_{\text{new}}))$ 
14:   $loss = \lambda dloss + rloss$ 
15:   $\theta^* = \text{ADAM\_OPTIMIZER}(\theta^*, loss)$ 
16:   $\phi^* = \text{ADAM\_OPTIMIZER}(\phi^*, loss)$ 
17:   $i = i + 1$ 
18: end for
19:
20: return  $\theta^*, \phi^*$ 

```

1) *Distortion Alleviation Using Finetuned Model:* The subplots at second row of both Fig. 8b and 8c visualize adversarial reconstructions of the same adversarial input by respectively applying pretrained and finetuned Ballé 2018 model. As for comparative study, we also plot the original input (without attack) and its decoded reconstruction using the pretrained NIC model at the first and second rows of Fig. 8a. As seen, adversarially-finetuned NIC model can effectively defend noise perturbation augmented in input image, for which we believe it is because the pretrained NIC model is improved by adversarial finetuning to better characterize the distribution of noisy input.

In Fig. 8a and 8b, we also picture the compressed latent features $\mathbf{z} = f_E(\mathbf{x})$ of the original image and adversarial input by baseline model. Here we choose the channel that is spatially most correlated with the output distortion. Noticeable variations in features confirm the insufficient capacity of native, pretrained baseline model to model and reconstruct these perturbations. Specifically, Fig. 8d gives the overall distribution comparison in latent feature space between original input and adversarial input using the baseline model. As we can see, feature distributions are almost the same for some channels like the 17-th, 37-th and 149-th channels, while they are very different for some channels like the 41-st, 124-th and 136-th channels, demonstrating the capability of the adversarial examples to enrich the distribution of the original dataset. Therefore, by finetuning the baseline model with these augmented adversarial examples, we can extend the model representative capacity to effectively reconstruct the

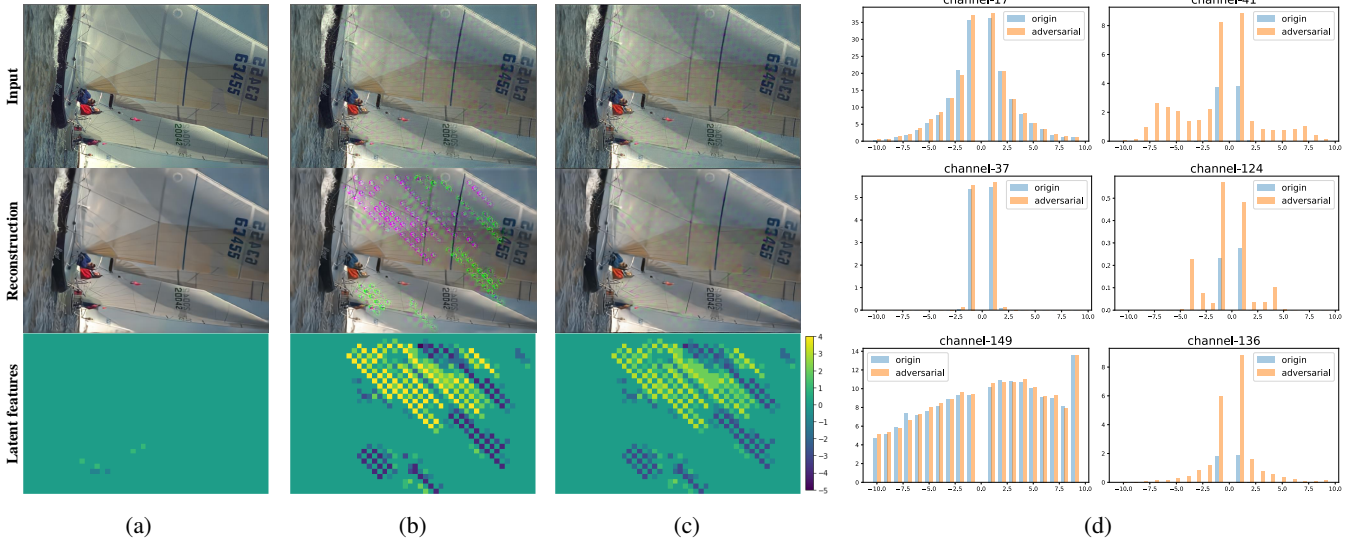


Fig. 8: **Attack Defense Using Adversarially-Finetuned Model.** (a) Original (noise-free) input, decoded reconstruction using pretrained NIC model, and 41th channel response of compressed latent features; (b) Adversarial input, adversarial reconstruction using pretrained NIC model, and 41th channel response of compressed latent features; (c) Adversarial input, adversarial reconstruction using adversarially finetuned NIC model, and 41th channel response of compressed latent features; The reconstruction without adversarial finetuning in (b) exhibits severe distortion; while the distortion in decoded reconstruction using finetuned NIC model in (c) is greatly alleviated and removed. Note that the latent features are presented at a size of $1/16 \times 1/16$ of the original image, they are upscaled for better visualization. (d) Distribution comparison in latent space between original input and adversarial input coded using pretrained model. For some channels (e.g. 17-th, 37-th, 149-th), they are very similar. However, latent features in 41-st, 124-th, 136-th, present quite distant distribution. For better visualization, feature elements with value 0 are removed.

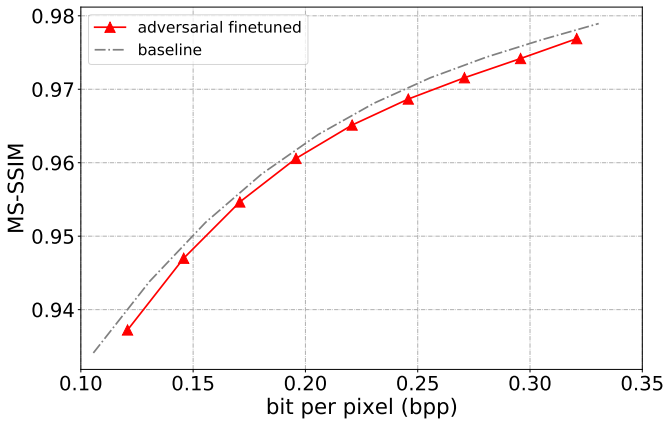


Fig. 9: **Coding Efficiency.** Rate-distortion efficiency averaged using total 24 Kodak images for pretrained baseline model (a.k.a., Ballé 2018 [2]), and finetuned model using generated adversarial examples from DIV2K dataset \mathbb{D} .

perturbation. As shown in Fig. 8c, with similar response in latent features as in Fig. 8b, the reconstruction distortion is greatly alleviated.

More importantly, we then attempt to generate new adversarial examples to attack the finetuned NIC model. Experiment results in Tab. IV report the effective defense of these attacks without noticeable distortion in adversarial reconstructions, further revealing the improved robustness of underlying model

with proposed methodology.

TABLE IV: Adversarial reconstruction quality comparison between baseline model and adversarial finetuned model averaged on Kodak dataset. The reconstruction quality is significantly improved for model that finetuned on adversarial examples.

Methods	PSNR (dB)	MS-SSIM
Balle 2018 MS-SSIM opt. (baseline model)	11.6085	0.6752
finetuned model	23.7074	0.9064

2) *Coding Efficiency of Finetuned Model:* Previous discussions show that finetuned compression model can effectively defense noise attacks. Another important question then arises: whether the coding efficiency of finetuned model is retained.

To better understand this question, we perform a comparative study using two models:

- Baseline Model: native, pretrained Ballé 2018 model, provided by compressAI [41];
- Adversarial Finetuned Model: finetuning the pretrained baseline using generated adversarial examples.

We then use these models to independently encode 24 Kodak images and measure the average rate-distortion efficiency. As in Fig. 9, the coding efficiency of finetuned model shows only slight drop compared with the baseline model, revealing that adversarial finetuning could not only effectively improve the model robustness, but also clearly retain the coding efficiency as the original model. This reports that

our methodology is a quick plug-and-play strategy without requiring any changes to underlying compression framework, showing that our solution is simple, effective and generalizable to most existing neural image compression approaches.

C. Recompression Application

Image recompression is very common in applications. As reported in [16], successive recompression using learnt image coder would lead to severe distortion in reconstruction. To tackle it, Kim *et. al* [16] included images that were repeatedly compressed in training to improve the model robustness on purpose. Our proposed adversarial finetune strategy is not designed for any specific scenario. However, given that compression artifacts can also be treated as the additive noises, we then test the finetuned compression model on this recompression task.

The visual comparison using Kodak images is shown in Fig. 1. After 50 repetitions of recompression, severe distortions can be found in reconstructions encoded using pretrained compression model, while these unexpected distortions are completely eliminated or greatly alleviated in decoded images that were compressed using finetuned model. This clearly evidences the generalization of our method to real-life applications like image recompression. We also expect that our methodology can be applied to other pixel domain regression tasks for robustness evaluation and improvement in future works such as quality enhancement, super resolution, etc..

VI. EXTENDING THE METHODOLOGY TO TARGETED ATTACK

This companion section showcases that our methodology can be also applied to targeted attack. Different from the untargeted attack in previous sections that tends to just maximize the reconstruction distortion, A targeted attack is typically applied for semantic content understanding, which attempts to produce a targeted output that is designated to be different from the original output.

A. Targeted Adversarial Examples

Assuming that we have the source image \mathbf{x} and a target image \mathbf{x}^t that is different from \mathbf{x} , we hope to generate adversarial input $\mathbf{x}^* = \mathbf{x} + \mathbf{n}$, so that the reconstructed $\hat{\mathbf{x}}^* = f_D(f_E(\mathbf{x}^*))$ would be close to the reconstruction of the target image $\hat{\mathbf{x}}^t = f_D(f_E(\mathbf{x}^t))$. By fixing the encoder $f_E()$ and decoder $f_D()$ of a specific NIC method, the generation of adversarial examples for targeted attack can be formulated as minimizing the input noise as well as the output distance with the target output:

$$\arg \min_{\mathbf{n}} L_t = \begin{cases} \|\mathbf{n}\|_2^2, & \|\mathbf{n}\|_2^2 \geq \epsilon \\ \|\hat{\mathbf{x}}^* - \hat{\mathbf{x}}^t\|_2^2, & \|\mathbf{n}\|_2^2 < \epsilon \end{cases} \quad (7)$$

Similar to (5), here ϵ is the threshold of the input noise to control the perturbation level. The main difference between targeted attack in (7) and untargeted attack in (5) is that: instead of using negative l_2 distance that maximizes the output distortion as in (5), here the objective is to minimize the

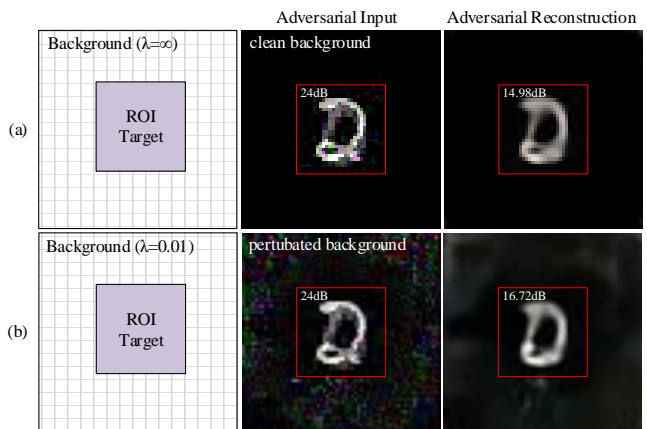


Fig. 10: **Attack with target area mask.** (a) example of adversarial attack with masked ROI (region of interest) target. Zero perturbation is added in the background area. (b) perturbations are added in both target area and background area with $\lambda = 0.01$ in (8). With same level of target area input perturbation, the attack efficiency is further improved by allowing some extra perturbation in the background area.

distance between the reconstruction of target image $\hat{\mathbf{x}}^t$ and the reconstruction of the adversarial example $\hat{\mathbf{x}}^*$.

Note that (7) simply hopes to minimize the distance between source image and target image of all pixels, which works well for low-resolution, thumbnail images, such as the handwritten digits dataset MNIST. Nowadays, an image often exhibits at a much higher spatial resolution, such as the 4K, 8K, etc, and usually present multiple semantic cues, e.g., diverse foreground objects, within the same scene, making it difficult to directly apply the (7). For most real-life images, we then suggest a more practical strategy that focuses on alerting salient object or area (e.g. text, face, etc) that is attentive to human observers. The target in an image usually occupies a small fraction of the entire scene, thus we can simply mask out the target area manually or by any target segmentation / saliency detection algorithms, while keeping the background unchanged as in Fig. 10(a).

Considering that the stacked convolution layers and resolution resampling used in most NIC solutions would enlarge the receptive field of the network, it implies that the perturbation added in surrounding background area would also potentially affect the reconstruction of the target area. To fit the general use cases, we still assume that the noise can be added to the entire image, but set different weights in target area \mathbf{x}_{roi} and background area \mathbf{x}_{bkg} in optimization, e.g.,

$$\begin{aligned} & \arg \min_{\mathbf{n}} L_t \\ & = \begin{cases} \|\mathbf{x}_{\text{roi}}, \mathbf{x}_{\text{roi}}^*\|_2^2 + \lambda \|\mathbf{x}_{\text{bkg}}, \mathbf{x}_{\text{bkg}}^*\|_2^2, & \|\mathbf{n}_{\text{roi}}\|_2^2 \geq \epsilon, \\ \|\hat{\mathbf{x}}_{\text{roi}}^* - \hat{\mathbf{x}}_{\text{roi}}^t\|_2^2 + \lambda \|\hat{\mathbf{x}}_{\text{bkg}}^* - \hat{\mathbf{x}}_{\text{bkg}}^t\|_2^2, & \|\mathbf{n}_{\text{roi}}\|_2^2 < \epsilon. \end{cases} \end{aligned} \quad (8)$$

Here the \mathbf{n}_{roi} and ϵ are the noise added in target area and its threshold. If $\lambda = \infty$ as in Fig. 10(a), Equation (8) is degenerated to (7) that no noise is allowed in the background area. Having a smaller λ that allows some perturbation in the

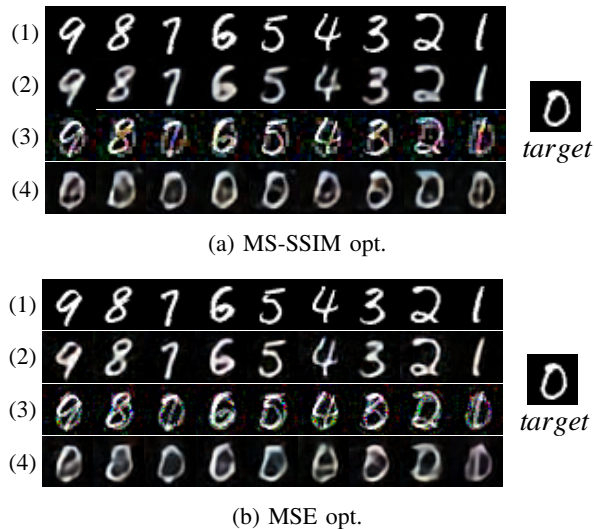


Fig. 11: Targeted adversarial examples and reconstructed output of MNIST [48] samples compressed using (a) MS-SSIM loss optimized NIC model; and (b) MSE loss optimized NIC model; (1) original source images, (2) decoded reconstructions of original images, (3) adversarial examples, (4) adversarial reconstructions. Same target image is shown on the right for both MSE and MS-SSIM optimized image compression model.

background area can improve the attack efficiency as shown in Fig. 10(b).

B. Attack Evaluation

Adversarial examples generated with the optimization function described in (7) on MNIST dataset are shown in Fig. 11. Note that original MNIST dataset are composed of single channel grayscale images. To feed them into image compression models that normally input 3-channel RGB color images, we duplicate them to 3 channels with equal values. Experiment results show that by injecting noise perturbation to input image as in (7), the adversarial reconstruction significantly differs from the original input and is visually even closer to the designated target. Both MSE and MS-SSIM optimized compression models are vulnerable to such targeted attack.

A high-resolution large-scale dataset Cityscapes [49] that contains a diverse set of stereo videos recorded in street scenes from 50 different cities, is also tested to demonstrate the effectiveness of targeted adversarial attacks with area masking on car plate. We apply (8) to generate targeted adversarial examples where we set $\lambda = 0.1$. As shown in Fig. 12, the numbers in car plate can be successfully modified to have the adversarial reconstruction closer to the designated target, which may consequently affect the inference engine for decision-making in autonomous driving and surveillance. The impact of image resolution is also tested, showing the same effectiveness of targeted attack at different resolutions.

C. Application Limitations

First, similar to the defense strategy in Sec. V, we can also include targeted adversarial examples into the training



Fig. 12: Targeted adversarial attack on Cityscapes dataset with plate ROI mask. The license plate number area is marked in red box as the target area. Masked patches at native resolution 240×240 and downscaled resolution with a factor of 2 at each dimension (120×120) are both tested. Plots are scaled to the same size for better visualization.

stage to finetune the model for improved robustness. However, in real-life applications, the “target” of adversarial attack in pixel domain is abundant, making it impossible to include all potential “targets”. A more practical solution for the defense of targeted attack is to limit the methodology developed in this work to some specific task.

Besides, we mainly focus on pixel-wise attack that affects the reconstruction visually in this paper. Another important domain of adversarial attack is to fool the artificial system (e.g. the accuracy of face recognition system) instead of human eyes. We leave the problem of the defense of targeted attack and the attack of NIC solutions in computer vision tasks for future study.

VII. CONCLUSION

In this paper, we propose to generate adversarial examples to examine the model robustness of existing learnt image compression methods. Experiments show that all tested methods are vulnerable to adversarial attack regardless of their network architectures, loss functions, and quality settings. To tackle it, we then propose to include adversarial examples to finetune the underlying models. Results have shown the effectiveness of our methodology, not only successfully defending the adversarial attack with great distortion alleviation in reconstruction, but also retaining the outstanding compression performance. It is also demonstrated that our methodology can be easily extended to targeted attack. Our proposed method is generalizable to most popular learnt image compression frameworks,

and can be applied to other pixel domain regression tasks as well in future work.

VIII. ACKNOWLEDGEMENT

We are very grateful for the authors [1], [2], [4]–[7], [34] who have made their learning-based image compression methods open source to public.

REFERENCES

- [1] J. Ballé, V. Laparra, and E. P. Simoncelli, “End-to-end optimized image compression,” *arXiv preprint arXiv:1611.01704*, 2016. 1, 3, 4, 6, 12
- [2] J. Ballé, D. Minnen, S. Singh, S. J. Hwang, and N. Johnston, “Variational image compression with a scale hyperprior,” *arXiv preprint arXiv:1802.01436*, 2018. 1, 3, 4, 5, 6, 7, 9, 12
- [3] M. Li, W. Zuo, S. Gu, D. Zhao, and D. Zhang, “Learning convolutional networks for content-weighted image compression,” in *Proceedings of the IEEE Conference on Computer Vision and Pattern Recognition*, 2018, pp. 3214–3223. 1
- [4] D. Minnen, J. Ballé, and G. D. Toderici, “Joint autoregressive and hierarchical priors for learned image compression,” in *Advances in Neural Information Processing Systems*, 2018, pp. 10 794–10 803. 1, 3, 4, 5, 6, 12
- [5] F. Mentzer, G. Toderici, M. Tschannen, and E. Agustsson, “High-fidelity generative image compression,” *arXiv preprint arXiv:2006.09965*, 2020. 1, 4, 5, 12
- [6] Z. Cheng, H. Sun, M. Takeuchi, and J. Katto, “Learned image compression with discretized gaussian mixture likelihoods and attention modules,” in *2020 IEEE/CVF Conference on Computer Vision and Pattern Recognition, CVPR 2020, Seattle, WA, USA, June 13-19, 2020*. IEEE, 2020, pp. 7936–7945. [Online]. Available: <https://doi.org/10.1109/CVPR42600.2020.00796> 1, 3, 4, 5, 6, 12
- [7] T. Chen, H. Liu, Z. Ma, Q. Shen, X. Cao, and Y. Wang, “End-to-end learnt image compression via non-local attention optimization and improved context modeling,” *IEEE Transactions on Image Processing*, vol. 30, pp. 3179–3191, 2021. 1, 3, 4, 5, 6, 12
- [8] Y. Hu, W. Yang, Z. Ma, and J. Liu, “Learning end-to-end lossy image compression: A benchmark,” *IEEE Transactions on Pattern Analysis and Machine Intelligence*, 2021. 1
- [9] M. Lu, P. Guo, H. Shi, C. Cao, and Z. Ma, “Transformer-based image compression,” *arXiv preprint arXiv:2111.06707*, 2021. 1
- [10] G. K. Wallace, “The jpeg still picture compression standard,” *Communications of the ACM*, vol. 34, no. 4, pp. 30–44, 1991. 1, 2
- [11] D. T. Lee, “Jpeg 2000: Retrospective and new developments,” *Proceedings of the IEEE*, vol. 93, no. 1, pp. 32–41, Jan 2005. 1, 2
- [12] B. Bross, J. Chen, J.-R. Ohm, G. J. Sullivan, and Y.-K. Wang, “Developments in international video coding standardization after avc, with an overview of versatile video coding (vvc),” *Proceedings of the IEEE*, pp. 1–31, 2021. 1
- [13] Z. Li, H. Liu, L. Yang, and Z. Ma, “In-camera raw compression: A new paradigm from image acquisition to display,” in *54th Asilomar Conference on Signals, Systems, and Computers, ACSSC 2020, Pacific Grove, CA, USA, November 1-4, 2020*, M. B. Matthews, Ed. IEEE, 2020, pp. 1132–1136. [Online]. Available: <https://doi.org/10.1109/IEEECONF51394.2020.9443315> 1
- [14] Z. Wang, E. P. Simoncelli, and A. C. Bovik, “Multiscale structural similarity for image quality assessment,” in *Signals, Systems and Computers, 2004. Conference Record of the Thirty-Seventh Asilomar Conference on*, vol. 2. Ieee, 2003, pp. 1398–1402. 1, 2
- [15] X. Wang, T. Chen, and Z. Ma, “Subjective quality optimized efficient image compression,” in *Proceedings of the IEEE/CVF Conference on Computer Vision and Pattern Recognition*, 2021, pp. 1911–1915. 1
- [16] J.-H. Kim, S. Jang, J.-H. Choi, and J.-S. Lee, “Instability of successive deep image compression,” ser. MM ’20. New York, NY, USA: Association for Computing Machinery, 2020, p. 247–255. [Online]. Available: <https://doi.org/10.1145/3394171.3413680> 1, 2, 10
- [17] J. Choi and B. Han, “Task-aware quantization network for jpeg image compression,” in *European Conference on Computer Vision*. Springer, 2020, pp. 309–324. 2
- [18] I. J. Goodfellow, J. Shlens, and C. Szegedy, “Explaining and harnessing adversarial examples,” in *3rd International Conference on Learning Representations, ICLR 2015, San Diego, CA, USA, May 7-9, 2015, Conference Track Proceedings*, 2015. 2, 3, 4
- [19] I. Goodfellow, J. Shlens, and C. Szegedy, “Explaining and harnessing adversarial examples,” in *International Conference on Learning Representations*, 2015. [Online]. Available: <http://arxiv.org/abs/1412.6572> 2, 8
- [20] A. Nguyen, J. Yosinski, and J. Clune, “Deep neural networks are easily fooled: High confidence predictions for unrecognizable images,” in *Proceedings of the IEEE conference on computer vision and pattern recognition*, 2015, pp. 427–436. 2
- [21] C. Xiao, R. Deng, B. Li, F. Yu, M. Liu, and D. Song, “Characterizing adversarial examples based on spatial consistency information for semantic segmentation,” in *Proceedings of the European Conference on Computer Vision (ECCV)*, September 2018. 2
- [22] X. Wei, S. Liang, N. Chen, and X. Cao, “Transferable adversarial attacks for image and video object detection,” in *Proceedings of the Twenty-Eighth International Joint Conference on Artificial Intelligence, IJCAI-19. International Joint Conferences on Artificial Intelligence Organization*, 7 2019, pp. 954–960. [Online]. Available: <https://doi.org/10.24963/ijcai.2019/134> 2
- [23] M. Yin, Y. Zhang, X. Li, and S. Wang, “When deep fool meets deep prior: Adversarial attack on super-resolution network,” in *Proceedings of the 26th ACM International Conference on Multimedia*, ser. MM ’18. New York, NY, USA: Association for Computing Machinery, 2018, p. 1930–1938. [Online]. Available: <https://doi.org/10.1145/3240508.3240603> 2
- [24] A. Ranjan, J. Janai, A. Geiger, and M. J. Black, “Attacking optical flow,” in *Proceedings of the IEEE International Conference on Computer Vision*, 2019, pp. 2404–2413. 2
- [25] R. Zhang, P. Isola, A. A. Efros, E. Shechtman, and O. Wang, “The unreasonable effectiveness of deep features as a perceptual metric,” in *Proceedings of the IEEE conference on computer vision and pattern recognition*, 2018, pp. 586–595. 2, 4, 7
- [26] K. He, X. Zhang, S. Ren, and J. Sun, “Deep residual learning for image recognition,” in *Proceedings of the IEEE conference on computer vision and pattern recognition*, 2016, pp. 770–778. 3
- [27] J. Ballé, V. Laparra, and E. P. Simoncelli, “Density modeling of images using a generalized normalization transformation,” *arXiv preprint arXiv:1511.06281*, 2015. 3
- [28] N. Ahmed, T. Natarajan, and K. R. Rao, “Discrete cosine transform,” *IEEE transactions on Computers*, vol. 100, no. 1, pp. 90–93, 1974. 2
- [29] B.-F. Wu and C.-F. Lin, “A high-performance and memory-efficient pipeline architecture for the 5/3 and 9/7 discrete wavelet transform of jpeg2000 codec,” *IEEE Transactions on circuits and systems for video technology*, vol. 15, no. 12, pp. 1615–1628, 2005. 2
- [30] J. Zepeda, C. Guillemot, and E. Kijak, “Image compression using sparse representations and the iteration-tuned and aligned dictionary,” *IEEE Journal of Selected Topics in Signal Processing*, vol. 5, no. 5, pp. 1061–1073, 2011. 3
- [31] Y. Xue and Y. Wang, “Video coding using a self-adaptive redundant dictionary consisting of spatial and temporal prediction candidates,” in *2014 IEEE International Conference on Multimedia and Expo (ICME)*, 2014, pp. 1–6. 3
- [32] J. Lee, S. Cho, and S.-K. Beack, “Context-adaptive entropy model for end-to-end optimized image compression,” *arXiv preprint arXiv:1809.10452*, 2018. 3
- [33] L. Helminger, A. Djelouah, M. Gross, and C. Schroers, “Lossy image compression with normalizing flows,” in *Neural Compression: From Information Theory to Applications – Workshop @ ICLR 2021*, 2021. [Online]. Available: <https://openreview.net/forum?id=NQJ9pMF9id> 3, 7
- [34] Y. Xie, K. L. Cheng, and Q. Chen, “Enhanced invertible encoding for learned image compression,” in *Proceedings of the ACM International Conference on Multimedia*, 2021. 3, 4, 6, 12
- [35] W. Hong, T. Chen, M. Lu, S. Pu, and Z. Ma, “Efficient neural image decoding via fixed-point inference,” *IEEE Transactions on Circuits and Systems for Video Technology*, vol. 31, no. 9, pp. 3618–3630, 2021. 4, 6
- [36] D. P. Kingma and J. Ba, “Adam: A method for stochastic optimization,” *arXiv:1412.6980v9*, Jan. 2017. 4
- [37] P. Tabacof, J. Tavares, and E. Valle, “Adversarial images for variational autoencoders,” *ArXiv*, vol. abs/1612.00155, 2016. 4
- [38] J. Kos, I. Fischer, and D. Song, “Adversarial examples for generative models,” in *2018 IEEE Security and Privacy Workshops (SPW)*. IEEE, 2018, pp. 36–42. 4
- [39] A. B. L. Larsen, S. K. Sønderby, H. Larochelle, and O. Winther, “Autoencoding beyond pixels using a learned similarity metric,” in *ICML’16 Proceedings of the 33rd International Conference on International Conference on Machine Learning - Volume 48*, 2016, pp. 1558–1566. 4

- [40] Y. Netzer, T. Wang, A. Coates, A. Bissacco, B. Wu, and A. Y. Ng, "Reading digits in natural images with unsupervised feature learning," 2011. 4
- [41] J. Bégin, F. Racapé, S. Feltman, and A. Pushparaja, "Compressai: a pytorch library and evaluation platform for end-to-end compression research," arXiv preprint arXiv:2011.03029, 2020. 6, 9
- [42] E. Kodak. Kodak lossless true color image suite (photocd pcd0992). [Online]. Available: <http://r0k.us/graphics/kodak/> 6
- [43] C. Huang, H. Liu, T. Chen, Q. Shen, and Z. Ma, "Extreme image coding via multiscale autoencoders with generative adversarial optimization," in 2019 IEEE Visual Communications and Image Processing (VCIP). IEEE, 2019, pp. 1–4. 7
- [44] C. Szegedy, W. Zaremba, I. Sutskever, J. Bruna, D. Erhan, I. Goodfellow, and R. Fergus, "Intriguing properties of neural networks," in International Conference on Learning Representations, 2014. [Online]. Available: <http://arxiv.org/abs/1312.6199> 8
- [45] R. Huang, B. Xu, D. Schuurmans, and C. Szepesvari, "Learning with a strong adversary," Computer Science, 2015. 8
- [46] A. Kurakin, D. Boneh, F. Tramèr, I. Goodfellow, N. Papernot, and P. McDaniel, "Ensemble adversarial training: Attacks and defenses," 2018. [Online]. Available: <https://openreview.net/pdf?id=rkZvSe-RZ> 8
- [47] E. Agustsson and R. Timofte, "Ntire 2017 challenge on single image super-resolution: Dataset and study," in The IEEE Conference on Computer Vision and Pattern Recognition (CVPR) Workshops, July 2017. 8
- [48] Y. Lecun, L. Bottou, Y. Bengio, and P. Haffner, "Gradient-based learning applied to document recognition," Proceedings of the IEEE, vol. 86, no. 11, pp. 2278–2324, 1998. 11
- [49] M. Cordts, M. Omran, S. Ramos, T. Rehfeld, M. Enzweiler, R. Benenson, U. Franke, S. Roth, and B. Schiele, "The cityscapes dataset for semantic urban scene understanding," in Proc. of the IEEE Conference on Computer Vision and Pattern Recognition (CVPR), 2016. 11